

diffusivities between the SCF and the catalyst surface and of reduced coke deposition, benefits that have no parallel in homogeneous catalysis. The restriction to nonpolar or weakly polar reactants has been overcome through the use of entrainers or surfactants. For example, DeSimone and others have cleverly used soluble fluoropolymers in small amounts as surfactants to achieve greater rates or uniformity of product particle size during polymerization of methylmethacrylate (47) or acrylamide (48) in $scCO_2$. A similar approach could be used for molecularly catalyzed polar reactions in $scCO_2$.

The industrial outlook for SCFs as reaction media may be favorable because of the beneficial environmental effect of dispensing with organic liquid solvents. High-pressure operations would be facilitated in large-scale production processes and especially continuous-flow systems for which SCFs are well suited. Because of the non-toxicity of $scCO_2$, a future direction for molecular catalysis in that medium could be pharmaceutical synthesis. This is a field in which homogeneous transition metal-based catalysts have had a great impact. It is certain that researchers of homogeneous catalysis will adopt SCF as media for many more reactions and thus broaden the scope of this technique.

REFERENCES AND NOTES

- R. Noyori, *Science* **248**, 1194 (1990).
- _____, *Asymmetric Catalysis in Organic Synthesis* (Wiley, New York, 1994).
- B. Subramaniam and M. A. McHugh, *Ind. Eng. Chem. Process Des. Dev.* **25**, 1 (1986).
- J. F. Brennecke, *ACS Symp. Ser.* **514**, 201 (1993).
- E. Kiran and J. M. H. Levelt Sengers, Eds., *Supercritical Fluids Fundamentals for Application*, vol. 273 of the NATO ASI Series E (Kluwer Academic, Dordrecht, Netherlands, 1994).
- G. M. Kramer and F. Leder, U.S. Patent 3 880 945 (1975).
- J. W. Rathke, R. J. Klingler, T. R. Krause, *Organometallics* **10**, 1350 (1991).
- P. G. Jessop, T. Ikariya, R. Noyori, *Nature* **368**, 231 (1994).
- K. P. Johnston and C. Haynes, *AIChE J.* **33**, 2017 (1987).
- S. Kim and K. P. Johnston, *ACS Symp. Ser.* **329**, 42 (1987).
- R. W. Shaw, T. B. Brill, A. A. Clifford, C. A. Eckert, E. U. Franck, *Chem. Eng. News* **69** (no. 51), 26 (1991).
- G. J. Tawa and L. R. Pratt, *J. Am. Chem. Soc.* **117**, 1625 (1995).
- K. D. Bartle, A. A. Clifford, S. A. Jafar, G. F. Shilstone, *J. Phys. Chem. Ref. Data* **20**, 713 (1991).
- M. E. Sigman, S. M. Lindley, J. E. Leffler, *J. Am. Chem. Soc.* **107**, 1471 (1985).
- Y. Ikushima, N. Saito, M. Arai, *J. Phys. Chem.* **96**, 2293 (1992).
- J. A. Hyatt, *J. Org. Chem.* **49**, 5097 (1984).
- C. Reichardt, *Chem. Rev.* **94**, 2319 (1994).
- D. K. Dandge, J. P. Heller, K. V. Wilson, *Ind. Eng. Chem. Prod. Res. Dev.* **24**, 162 (1985).
- P. G. Jessop, Y. Hsiao, T. Ikariya, R. Noyori, *J. Am. Chem. Soc.* **116**, 8851 (1994).
- R. J. Klingler and J. W. Rathke, *ibid.*, p. 4772.
- Their work has been reviewed: M. Poliakoff and S. Howdle, *Chem. Br.* **1995**, 118 (1995).
- S. M. Howdle, M. A. Healy, M. Poliakoff, *J. Am. Chem. Soc.* **112**, 4804 (1990), and references therein.

- J. A. Banister *et al.*, *J. Organomet. Chem.* **484**, 129 (1994).
- J. A. Banister, S. M. Howdle, M. Poliakoff, *Chem. Commun.* **1993**, 1814 (1993).
- M. Jobling *et al.*, *ibid.* **1990**, 1287 (1990).
- M. Jobling *et al.*, *ibid.*, p. 1762.
- M. J. Clarke *et al.*, *Inorg. Chem.* **32**, 5643 (1993).
- P. G. Jessop, T. Ikariya, R. Noyori, *Organometallics* **14**, 1510 (1995).
- J. M. DeSimone, Z. Guan, C. S. Elsbernd, *Science* **257**, 945 (1992).
- Z. Guan, J. R. Combes, Y. Z. Menciloglu, J. M. DeSimone, *Macromolecules* **26**, 2663 (1993).
- J. E. Cottle, U.S. Patent 3 294 772 (1966).
- B. Folie and M. Radosz, in *Proceedings of the Third International Symposium on Supercritical Fluids* (Strasbourg, France, 17 to 19 October 1994), pp. 281-286.
- M. T. Reetz *et al.*, *Chimia* **47**, 493 (1993).
- Y. Inoue, Y. Itoh, H. Kazama, H. Hashimoto, *Bull. Chem. Soc. Jpn.* **53**, 3329 (1980).
- T. Ikariya, P. G. Jessop, R. Noyori, Japanese Patent Appl. 274721 (1993).
- P. G. Jessop, Y. Hsiao, T. Ikariya, R. Noyori, *Chem. Commun.* **1995**, 707 (1995).
- J. Xiao, S. C. A. Nefkens, P. G. Jessop, T. Ikariya, R. Noyori, in preparation.

- T. Ohta *et al.*, *J. Org. Chem.* **52**, 3174 (1987).
- X. Zhang *et al.*, *Synlett* **1994**, 501 (1994).
- J. W. Rathke, R. J. Klingler, T. R. Krause, *Organometallics* **11**, 585 (1992); J. W. Rathke and R. J. Klingler, U.S. Patent 5 198 589 (1993).
- H. H. Yang and C. A. Eckert, *Ind. Eng. Chem. Res.* **27**, 2009 (1988).
- K. S. Jerome and E. J. Parsons, *Organometallics* **12**, 2991 (1993).
- O. Aaltonen and M. Rantakylä, *Chemtech* **21**, 240 (1991).
- A. J. Russell *et al.*, *ibid.* **24**, 33 (1994).
- M. Buback, *Angew. Chem. Int. Ed. Engl.* **30**, 641 (1991).
- G. Kaupp, *ibid.* **33**, 1452 (1994).
- J. M. DeSimone *et al.*, *Science* **265**, 356 (1994).
- F. A. Adamsky and E. J. Beckman, *Macromolecules* **27**, 312 (1994).
- R. C. Reid, J. M. Prausnitz, B. E. Poling, *The Properties of Gases and Liquids* (McGraw-Hill, New York, ed. 4, 1987).
- S. Angus, B. Armstrong, K. M. de Reuck, Eds., *International Thermodynamic Tables of the Fluid State: Carbon Dioxide* (Pergamon, Oxford, 1976).
- We gratefully acknowledge the assistance and advice of Y. Hsiao, J. Xiao, and K. Aoyagi of ERATO.

RESEARCH ARTICLE

Structures of Metal Sites of Oxidized Bovine Heart Cytochrome c Oxidase at 2.8 Å

Tomitake Tsukihara, Hiroshi Aoyama, Eiki Yamashita, Takashi Tomizaki, Hiroshi Yamaguchi, Kyoko Shinzawa-Itoh, Ryosuke Nakashima, Rieko Yaono, Shinya Yoshikawa*

The high resolution three-dimensional x-ray structure of the metal sites of bovine heart cytochrome c oxidase is reported. Cytochrome c oxidase is the largest membrane protein yet crystallized and analyzed at atomic resolution. Electron density distribution of the oxidized bovine cytochrome c oxidase at 2.8 Å resolution indicates a dinuclear copper center with an unexpected structure similar to a [2Fe-2S]-type iron-sulfur center. Previously predicted zinc and magnesium sites have been located, the former bound by a nuclear encoded subunit on the matrix side of the membrane, and the latter situated between heme a_3 and Cu_A , at the interface of subunits I and II. The O_2 binding site contains heme a_3 iron and copper atoms (Cu_B) with an interatomic distance of 4.5 Å; there is no detectable bridging ligand between iron and copper atoms in spite of a strong antiferromagnetic coupling between them. A hydrogen bond is present between a hydroxyl group of the hydroxyfarnesylethyl side chain of heme a_3 and an OH of a tyrosine. The tyrosine phenol plane is immediately adjacent and perpendicular to an imidazole group bonded to Cu_B , suggesting a possible role in intramolecular electron transfer or conformational control, the latter of which could induce the redox-coupled proton pumping. A phenyl group located halfway between a pyrrole plane of the heme a_3 and an imidazole plane liganded to the other heme (heme a) could also influence electron transfer or conformational control.

Bovine heart cytochrome c oxidase is a large multicomponent membrane protein complex with molecular size of 200 kilodaltons comprising 13 different polypeptide subunits. Located in the subunits are two heme A moieties, two redox active copper sites, one zinc, one magnesium, and possibly

some phospholipids as the intrinsic constituents (1, 2). This enzyme is one of the most intriguing biological macromolecules in the cell. As the terminal enzyme of biological oxidation, it reduces O_2 to H_2O at an active site with the four redox active transition metals coupling to a proton pumping pro-

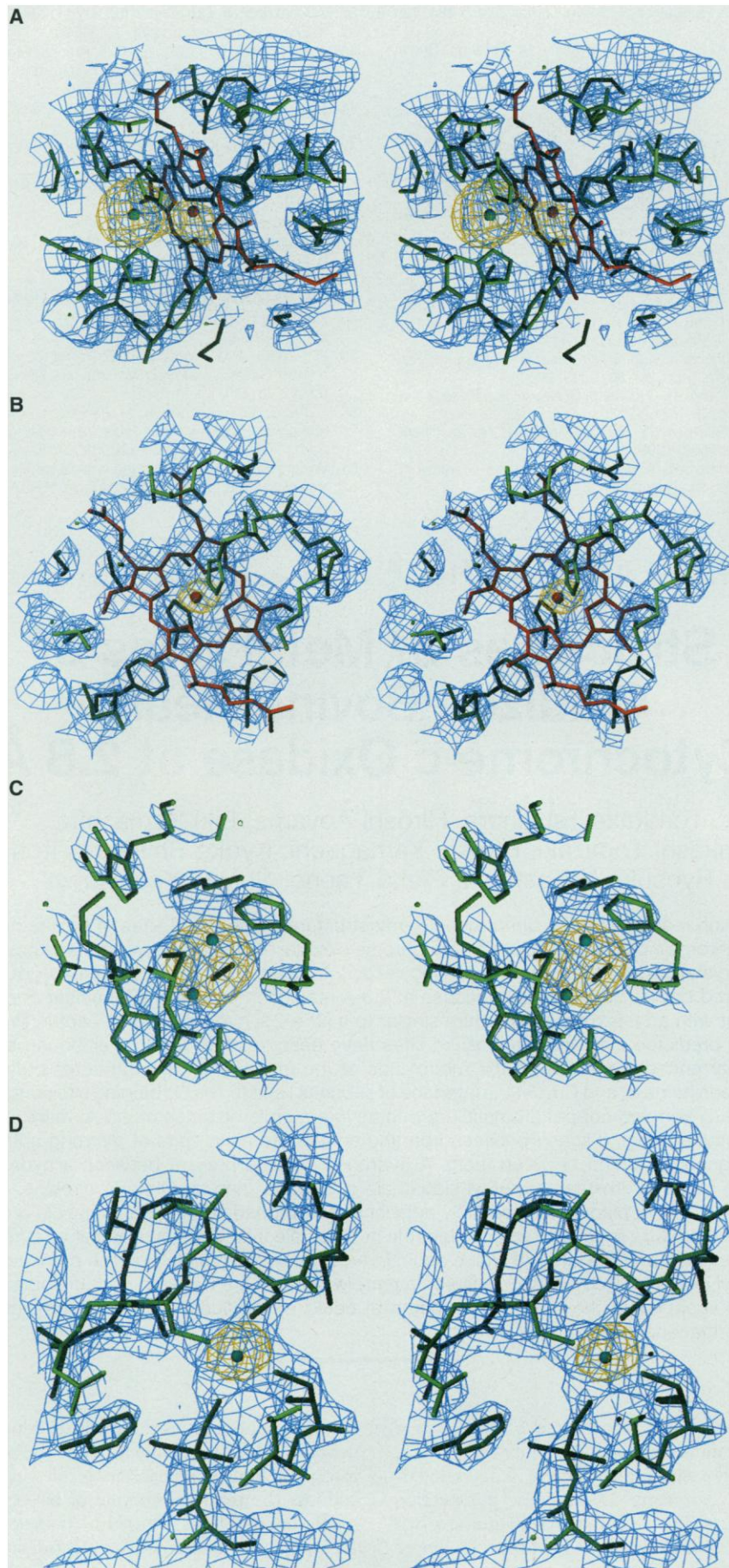


Fig. 1. Stereo pairs of the metal centers fitted in blue cages composed at 2σ of electron density at 2.8 \AA resolution together with yellow or brown cages, drawn at 10σ , of the native anomalous difference Fourier at 4.5 \AA resolution. Model fitting was performed by the programs Turbo Frodo (31) and X-FIT in the program package QUANTA (CTC Laboratory Systems Co., Ltd.) on SGI workstations. **(A)** The oxygen binding and reduction site. The heme a_3 shown in red bars and a red ball, Cu_B in a green ball, and the amino acid residues in green bars are fitted well in the cages. **(B)** The heme a , two histidine ligands of Fe_a , and some amino acid residues are shown in the same colors as in (A). **(C)** Dinuclear structure of the Cu_A . Two copper atoms are shown with brown balls, amino acid residues with green bars, and tetrahedral coordination of each copper atom in blue dotted lines. **(D)** Tetrahedral coordination structure of the zinc site. Four cysteines and zinc atom position are shown with green bars and a dark yellow ball, respectively.

cess across the mitochondrial inner membrane (2, 3). The bright green color of the enzyme, which is due to the heme iron and which changes sensitively with the redox and ligand-binding states of the active center, has stimulated electronic, resonance Raman, and infrared spectroscopic studies on its kinetic behavior during the enzymatic turnover (2-4).

Electron spin resonance studies have been made on the paramagnetic iron and copper ions (2, 3), and infrared spectroscopy has been used to study various respiratory inhibitors as probes for the O_2 binding site (5). In addition, the varied roles of the large and complex protein moiety, which in the mammalian enzyme contains 13 different polypeptide subunits with 3 being coded by a mitochondrial and nuclear genes and 10 by a nuclear gene, have been widely studied (1, 6). Thus, among the enzymes participating in biological oxidation, this one has been of primary interest ever since it was discovered (7). Despite these extensive and successful efforts, the absence of a crystal structure and analysis at atomic resolution has set limits on our understanding of the reaction mechanism of this enzyme. We had previously crystallized the enzyme from bovine heart, thus providing an example of x-ray diffractable crystals of a membrane protein isolated from a higher animal. However, the resolution of the crystals was far lower than suitable for x-ray structural analysis at atomic resolution (8). We therefore changed our techniques and have now ob-

T. Tsukihara, H. Aoyama, E. Yamashita, T. Tomizaki, and H. Yamaguchi are at the Institute for Protein Research, Osaka University, 3-2 Yamada-oka, Suita 565, Japan. K. Shinzawa-Itoh, R. Nakashima, R. Yaono, and S. Yoshikawa are at the Department of Life Science, Himeji Institute of Technology, Kamigohri Akoh, Hyogo 678-12, Japan.

*To whom correspondence should be addressed.

Table 1. Peak heights in the native electron density map at 2.8 Å and those in the anomalous difference Fourier map at 4.5 Å resolution.

Atomic group	Peak heights in σ unit	
	Electron density map	Anomalous difference map
Cu _A	12.1	14.3
Zn	10.9	9.7
Cu _B	11.4	9.3
Fe _{a₃}	10.3	5.1
Fe _a	10.0	5.3
PO ^{4*}	9.6	
PO ^{4*}	9.3	
PO ^{4*}	8.3	
Other highest	7.8	3.5

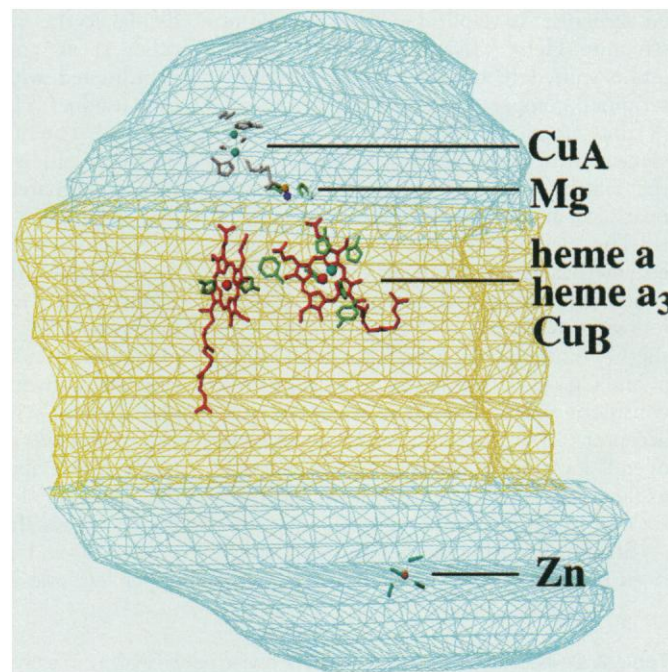
*PO⁴ represents a phosphate group of phospholipid.

tained crystals that diffract up to 2.6 Å resolution. During these procedures, it was necessary to adjust the structure of detergent that we used to stabilize the enzyme molecule in aqueous solution (9). We have now obtained from the electron density at 2.8 Å resolution the structures of the metal centers, which provide electron transfer pathways and serve as key structures for proton pumping.

Crystallization and structural determination. The crystals used for our study were prepared from bovine heart cytochrome c oxidase at the fully (resting) oxidized state (9) by the method previously described (8, 10). Briefly, the purified protein was stabilized in aqueous solution with the nonionic detergent, 0.2 percent decyl maltoside in 40 mM sodium phosphate buffer, pH 6.8, and crystallized by the batch method from a solution where the protein concentration was 9.0 percent (w/v) at 4°C, and with polyethylene glycol 4000 (Sigma) being used as the precipitant. The crystals diffracted x-rays up to 2.6 Å resolution. This enzyme preparation reacted with cyanide monophasically, but not so rapidly as the enzyme under turnover conditions, indicating that it is the “fast” form (11).

We have obtained electron density of the enzyme at 2.8 Å resolution by the multiple isomorphous replacement (MIR) method; we then used a density modification procedure coupled with noncrystallographic symmetry (NCS) averaging. The electron density distribution obtained was so clear that all the metal center structures were easily built into the map (Fig. 1). The model building was performed with a modeling option REFINO of Turbo Frodo to fit each residue with standard dimensions in appropriate electron density cages. The final refinement comparing the obtained model and x-ray diffraction data has not yet been completed. However, the electron density distribution with extremely high reliability,

Fig. 2. A schematic representation of metal site location in beef heart cytochrome c oxidase. Molecular surface defined with the electron density map at 5 Å resolution is shown by the cage. The yellow, the upper light blue, and the lower light blue represent a transmembrane part with 48 Å thickness, a hydrophilic part protruding to the cytosolic side with 37 Å, and the other hydrophilic part with 32 Å in the matrix space, respectively. The three metal centers, Fe_a, Fe_{a₃} and Cu_B are located at the same level, 13 Å below the membrane surface on the cytosolic side. Another metal center, Cu_A, close to the molecular surface is 8 Å above the membrane surface level, and magnesium ion is at the membrane surface level. The distances of Cu_A-Fe_a, Cu_A-Fe_{a₃}, Cu_A-Mg, Fe_{a₃}-Fe_a, and Fe_{a₃}-Mg are 19 Å, 22 Å, 9 Å, 14 Å, and 15 Å, respectively.



evidenced by R_{free} factor of 0.258 at 2.8 Å resolution, allows quite satisfactory fitting of the atomic model to the electron density in most parts of the enzyme molecule, including the metal sites. It is remarkable that such a high accuracy of the electron density distribution has been obtained from such a large and multicomponent protein complex. The quality of the atomic model assignments is clearly shown by stereoscopic drawings of the model structures superimposed on electron density cages (Fig. 1).

The following results also indicate that the electron density distribution is plausible and thus reliable.

1) The order in peak height of the electron density map is consistent with the order in number of electrons of a group located at the corresponding peak (Table 1).

2) The anomalous difference Fourier map clearly revealed metal centers in spite of very low anomalous contribution from the metals compared with the structure factor of a whole molecule (Fig. 1 and Table 1). This is strong evidence of extremely high accuracy of phases and electron density.

3) Of 1850 amino acid residues, main chains of 1808 residues were successfully located in the map. More than 90 percent of side chains of nonglycine residues have reasonable electron density cages.

We now present the metal site structures of the enzyme at the fully (resting) oxidized state. Intensity data collection and phase determination are summarized in Table 2.

Overall location of metal sites. The membrane-embedded region evaluated from the start and end of the helices was 48 Å wide in the middle part of the molecule (Fig. 2). The direction of the molecules with respect to the cytosolic and matrix sides was estimated from the location of a copper site, Cu_A (see below), and the positions of the NH₂- and COOH-termini of peptide subunits. All the 13 subunits, each different from the other, were assigned in the crystal structure, which provides conclusive evidence that all these subunits are intrinsic constituents of the enzyme and that each is present in equimolar amount. This enzyme is in a dimeric state in the crystal, and there is no indication for strong interaction between the metal sites of each monomer. One of the redox active copper sites, Cu_A, was located in the third largest subunit, subunit II (6), which protrudes to the cytosolic side 8 Å above the membrane surface. The position of Cu_A, which is a dinuclear copper center (see below), is defined as the middle point between the two copper atoms. The other redox active metal centers, heme a, heme a₃, and Cu_B, the latter two of which constitute the O₂ binding and reduction site (2, 3), were bound to subunit I at an identical level approximately 13 Å below (or inside) the membrane surface at the cytosolic side. Twelve transmembrane helices were found in subunit I, as has been predicted from the amino acid sequence (1, 12). Although most of the helices in the crystal structure are longer than those predicted, the numbering of the helices for the predict-

ed structure is applicable for the crystal structure. Helix VII is two residues shorter and is shifted 10 residues toward the NH₂-terminal, compared to the helix predicted. A zinc atom was close to the molecular surface in a nuclear-coded subunit Vb on the matrix side. The magnesium site was near Cu_A at the interface of subunits I and II. The electron transfer path within the enzyme has essentially been established recently after long and extensive efforts as follows: cytochrome c → Cu_A → heme a → the O₂ binding sites, which includes heme a₃ and Cu_B (13). The location of Cu_A seems consistent with its role as the initial electron acceptor from cytochrome c. However, this overall location of the metal site does not exclude the possibility for a direct electron transfer from Cu_A to the heme a₃-Cu_B site.

Structures of two hemes and Cu_B sites. Both heme planes were essentially perpen-

dicular to the membrane plane facing each other at an angle of 104°. Heme a was coordinated with two imidazoles of histidine residues (His⁶¹ in helix II and His³⁷⁸ in helix X). The fifth ligand of heme a₃ was an imidazole of His³⁷⁶ in helix X, whereas Cu_B was coordinated by three imidazoles of His²⁴⁰ in helix VI and His²⁹⁰ and His²⁹¹, both in a nonhelical fragment between helices VII and VIII. These ligations are consistent with those proposed as a result of mutagenesis experiments (12). The heme a₃ plane was positioned so that the pyrrole ring with a hydroxyfarnesylethyl side chain and the one with a vinyl side group were placed at lower right and left sides, respectively, when viewed from the Cu_B side, with the cytosolic side being considered as the upside. Thus, the pyrrole with methyl and propionic acid groups was located at the upper left side and the one with a formyl

and propionic acid groups was located at the upper right. In the case of heme a, the pyrrole with a hydroxyfarnesylethyl side chain was at the lower left, viewed from the Cu_B side (Fig. 2). The hydroxyfarnesylethyl group of heme a was almost in the extended conformation, held by helices I, II, X, XI, and XII, and that of heme a₃ was twisted to

Table 2. Collection of data and statistics of phase determination. The crystals diffracted x-rays up to 2.6 Å resolution. The crystal of the enzyme belongs to the orthorhombic space group of *P*2₁2₁2₁ with unit cell dimensions *a* = 189.1 Å, *b* = 210.5 Å, and *c* = 178.6 Å, containing two molecules in an asymmetric unit. Intensity data were collected with monochromatized x-ray of 1.0 Å at the Photon Factory, Tsukuba, Japan, by means of a modified Weissenberg camera for macromolecules (24). Diffraction intensities were processed with the program DENZO (25). Searching more than 50 heavy atom derivatives with MAC Science imaging plate detector (DIP2000) on a Rigaku rotating anode x-ray generator (RU300), we yielded three derivative data sets available for phase determination. Two of three derivatives were prepared by soaking the crystals in Na₂IrCl₆ solutions at various concentrations. The third was a CH₃HgCl derivative. Heavy atom sites of each derivative were located by solving each difference Patterson function at 5 Å resolution. The heavy atom parameters of three derivatives were refined with the program MLPHARE (26) of the CCP4 program package. In that MIR (27) phase information was poor beyond 5 Å resolution, phases were extended from 5 to 2.8 Å in 200 small steps with the use of solvent flattening (28) by means of the program DM of CCP4. The protein mask during the phase extension was determined by the Wang method (28) with a sphere of 10 Å and 70 percent solvent content by volume. A free *R* factor (29) for 5 percent of the reflections in each shell was reduced from 0.53 to 0.28. The noncrystallographic symmetry relation between two molecules in an asymmetric unit was determined, and the correlation coefficient $\{\sum(\rho_1 - \langle\rho_1\rangle)(\rho_2 - \langle\rho_2\rangle)/\sum[(\rho_1 - \langle\rho_1\rangle)^2(\rho_2 - \langle\rho_2\rangle)^2]^{1/2}\}$ was as high as 0.78. The phase refinement procedure including NCS averaging (30) was undertaken, starting at 5 to 2.8 Å resolution. The free *R* factor and the correlation coefficient at the final stage were 0.26 and 0.92, respectively.

	Native	IrCl ₆ (I)	IrCl ₆ (II)	CH ₃ HgCl
Resolution ranges (Å)*	100–2.8 (2.9–2.8)	100–3.0 (3.2–3.0)	100–3.0 (3.1–3.0)	100–3.0 (3.1–3.0)
Observed reflections	518,054 (24,542)	319,358 (18,599)	381,828 (28,410)	328,484 (15,186)
Independent reflections	159,742 (13,074)	125,036 (11,545)	133,245 (14,008)	127,548 (9,396)
<i>I</i> / σ (<i>I</i>)	19.5 (2.2)	10.0 (1.4)	21.3 (2.7)	2.4 (1.5)
Averaged redundancy†	3.2 (1.9)	2.6 (1.6)	2.9 (2.0)	2.6 (1.6)
Completeness (‡)	90.1 (74.4)	86.3 (64.5)	93.0 (79.1)	88.3 (65.7)
<i>R</i> _{merge} §	7.8 (29.0)	9.0 (29.6)	6.2 (23.4)	8.5 (28.4)
<i>R</i> _{iso}		7.3 (11.6)	5.7 (8.7)	9.0 (11.4)
<i>R</i> _{Cullis} ¶		0.90 (0.97)	0.86 (0.97)	0.79 (0.95)
Phasing power#		0.38 (0.18)	0.54 (0.30)	0.74 (0.34)

*Figures in parentheses are given for the highest resolution shells. †Redundancy is the number of observed reflections for each independent reflection. ‡ $R_{\text{merge}} = \sum_i \sum_h |I(h,i) - \langle I(h) \rangle| / \sum_i \sum_h I(h,i)$, where *I*(*h*,*i*) is the intensity value of the *i*-th measurement of *h* and $\langle I(h) \rangle$ is the corresponding mean value of *I*(*h*) for all *i* measurements; the summation is over the reflections with *I*/ σ (*I*) larger than 1.0. || $R_{\text{iso}} = \sum |F_{\text{PH}} - F_{\text{P}}| / \sum F_{\text{PH}}$, where *F*_{PH} and *F*_P are the derivative and the native structure factor amplitudes, respectively. ¶ $R_{\text{Cullis}} = \sum |F_{\text{PH}} - F_{\text{P}}| / \sum |F_{\text{PH}} - F_{\text{P}}|$, where *F*_H(calc) is the calculated heavy atom structure factor. The summation is over the centric reflections only. #Phasing power is root-mean-square (rms) isomorphous difference divided by rms residual lack of closure.

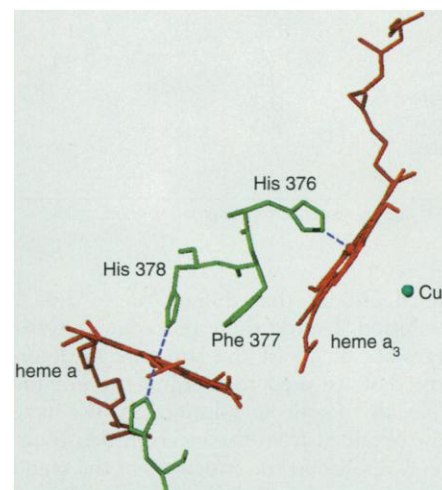


Fig. 3. Structural relation between two hemes in the active site of cytochrome c oxidase. Red structures and green structures represent hemes and amino acid residues in subunit I. A blue ball and red balls define the positions of copper and iron atoms, respectively. The hemes a and a₃ are bridged by three successive residues, His³⁷⁶, Phe³⁷⁷, and His³⁷⁸ in the helix X.

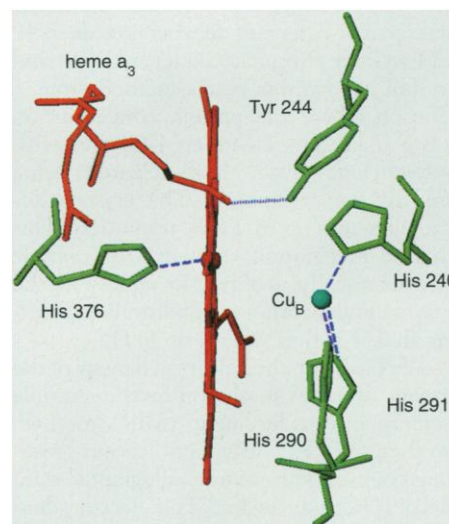


Fig. 4. A side view of the O₂ binding and reduction site. The red structure is heme a₃ and the green ones are amino acids. The dotted line shows a possible hydrogen bond between the hydroxyl of the hydroxyfarnesylethyl group and Tyr²⁴⁴. The broken lines represent coordination bonds. The red and green balls represent the positions of iron and copper atoms, respectively. A close contact between Tyr²⁴⁴ and His²⁴⁰ with both aromatic rings oriented perpendicular with each other is also shown.

form a U-shaped arm, located between helices VIII and IX. None of the hydroxyfarnesylethyl side chain interacted with the redox centers or the porphyrin aromatic ring system, contrary to the proposals based on the kinetic behavior of the enzyme (4, 14).

A phenyl plane of a phenylalanine (Phe³⁷⁷ in helix X) was observed halfway between the two planes of the heme a_3 and one of the imidazole ligands of heme a (His³⁷⁸) (Fig. 3). The distances between the phenyl plane and the two planes on both sides are as short as 3.5 Å. Thus, any change in the orientation and position of the phenyl group, induced by change in the ligation

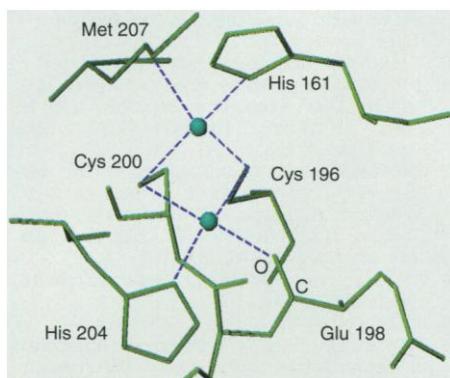


Fig. 5. A representation of Cu_A site showing a $[\text{2Cu-2S}\gamma]$ structure. Green balls show copper atom positions. Blue broken lines indicate coordination bonds. The peptide carbonyl group of Glu¹⁹⁸ is illustrated with a bar marked with C and O.

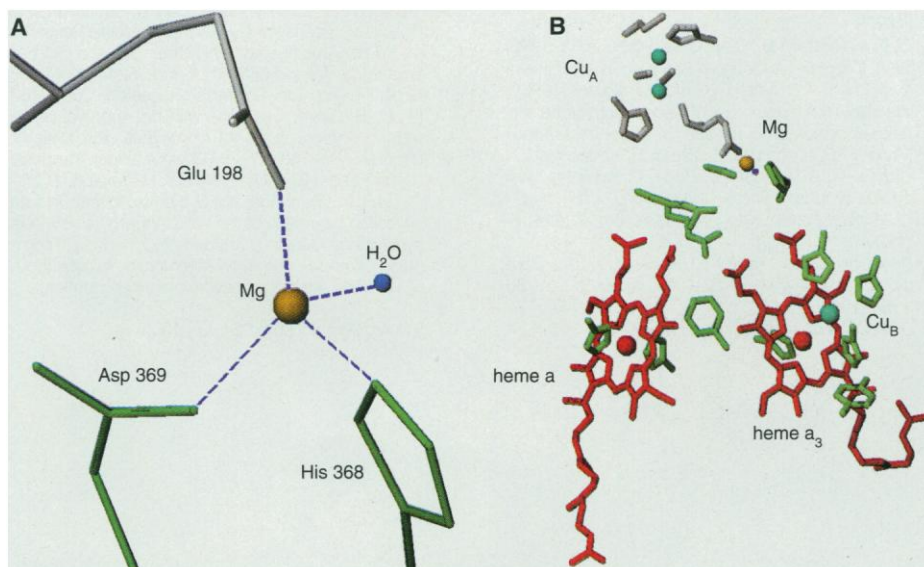


Fig. 6. The magnesium site and its relative orientation to other metal centers. **(A)** Coordination of magnesium. Green and light gray colors denote amino acid residues of subunits I and III, respectively. Dark orange and blue balls are at the positions of magnesium atom and oxygen atom of water, respectively. Blue broken lines are coordination bonds forming a distorted tetrahedron. **(B)** Location of the magnesium site and other active centers. Belonging of amino acids is shown with the same colors as in (A). Positions of iron, copper, magnesium, and oxygen of water are indicated with red, blue, dark orange, and dark blue balls, respectively.

and oxidation state of Fe_{a_3} from the fifth ligand imidazole of His³⁷⁶, adjacent to Phe³⁷⁷, could control the electron transfer between Fe_a and Fe_{a_3} .

A side view of the heme a_3 - Cu_B structure reveals the phenol OH group of tyrosine, Tyr²⁴⁴, in subunit I oriented to the OH of the hydroxyfarnesylethyl group (Fig. 4). The Cu_B site was coordinated only by the three imidazoles of His²⁴⁰, His²⁹⁰, and His²⁹¹. No other ligand to Cu_B , even water, was detected. The high spin Fe_{a_3} ion was slightly displaced from the heme plane toward the fifth ligand. The Cu_B was 4.5 Å away from Fe_{a_3} and 1.0 Å from the heme normal at Fe_{a_3} position toward the nitrogen atom of the pyrrole with the formyl group. One of the unexpected findings was the absence of a ligand directly bridging the Fe_{a_3} and Cu_B . A bridging ligand has been proposed on the basis of strong antiferromagnetic coupling between the two atoms, a characteristic that was discovered 26 years ago (15); other model structures with a bridging ligand have been proposed (16). The presence of an amino acid side chain randomly oriented so that the electron density could not be detected by x-ray crystallographic analysis is unlikely because all the amino acid side chains near the dinuclear site have been assigned. However, the presence of water molecules nonspecifically and randomly trapped cannot be excluded.

A typical hydrogen bond is likely to be present between the hydroxyl groups of a tyrosine (Tyr²⁴⁴) and the hydroxyfarnesylethyl side chain of heme a_3 in that the

oxygen-oxygen distance is 3.0 Å. Furthermore, the orientation of the phenol plane of Tyr²⁴⁴ was perpendicular to the imidazole plane of His²⁴⁰, which liganded to Cu_B . The nitrogen atom of the imidazole of His²⁴⁰ was located 3.1 Å above the plane of Tyr²⁴⁴. The system, including the imidazole phenol-hydroxyfarnesylethyl side chain, could facilitate an electron transfer pathway from Fe_{a_3} to Cu_B . A structure that could provide another electron transfer pathway from heme a_3 to Cu_B is the formyl side group at the pyrrole, located 3.0 Å above the imidazole plane of His²⁹⁰, which is a ligand of Cu_B . Although the distance between Fe_{a_3} and Cu_B , as short as 4.5 Å, suggests a facile electron transfer directly between the two metals, multiple electron transfer pathways are still possible for dioxygen reduction. In contrast, these structures may also induce an oxidation state-dependent conformational change to couple O_2 reduction with proton pumping. When Tyr²⁴⁴, which is not bound directly to Cu_B , was replaced by phenylalanine, Cu_B was disrupted (12), suggesting some structural role of the amino acid.

Other interesting structures near the heme a_3 and Cu_B site are a hydrogen bond between the imidazole of His³⁷⁶ (the fifth ligand of heme a_3) and the peptide carbonyl of Gly³⁵¹, and a parallel π - π contact between His²⁹¹ of Cu_B ligand and Trp²³⁶. The imidazole of a heme a ligand, His⁶¹, is linked to a carbonyl oxygen of Gly³⁰ with a hydrogen bond. No close contact with the formyl group of heme a is detectable.

Structure of Cu_A . The Cu_A site in subunit II consists of six ligands, two cysteines (Cys¹⁹⁶ and Cys²⁰⁰), two histidines (His¹⁶¹ and His²⁰⁴), a methionine (Met²⁰⁷), and a peptide carbonyl of a glutamate (Glu¹⁹⁸) (Fig. 5). All these ligands, except for the peptide carbonyl, have been proposed as a result of mutagenesis experiments (17). The anomalous Fourier map at the central metal site exhibited a single peak (Fig. 1), which suggested a single metal, although both the peak heights in the Fourier and the anomalous Fourier maps, respectively, were too high to be attributable to a single copper atom (Table 1). The arrangement of these six ligands, determined from the electron density distribution near this site, does not provide any reasonable position for a single copper atom, but is fully consistent with a dinuclear copper center, as follows. Two copper atoms are bridged by two sulfur atoms of Cys¹⁹⁶ and Cys²⁰⁰, placing the four atoms on the same plane with the interatomic distances of 2.7 Å (Cu-Cu), and 3.8 Å (Sγ-Sγ). One of the copper atoms is coordinated by the imidazole nitrogen of His¹⁶¹ and the methionine sulfur of Met²⁰⁷, forming a tetrahedral coordination including the two cysteine sulfur atoms. Coordination of the other copper is also tetrahe-

dral, including the imidazole nitrogen (His²⁰⁴) and the peptide carbonyl (Glu¹⁹⁸). The geometry is similar to that of a [2Fe-2S]-type iron-sulfur center (18), in which the Fe ions and inorganic sulfur atoms are replaced with Cu ions and cysteine sulfur atoms, respectively. Both dinuclear centers stabilize a one-electron delocalized oxidation state, that is, [Fe^{2.5+}---Fe^{2.5+}] in the reduced form of [2Fe-2S] center and [Cu^{1.5+}---Cu^{1.5+}] in the oxidized state of [2Cu-2S γ] center of Cu_A site. Recently, a dinuclear Cu center for Cu_A has been proposed in analogy to that of the copper enzyme N₂O reductase for which various structures not fully consistent with our structure have been suggested (19).

Structures of zinc and magnesium sites. Tetrahedral coordination was detectable for the zinc site where four cysteines (Cys⁶⁰, Cys⁶², Cys⁸², and Cys⁸⁵) in subunit Vb are coordinated by the central atom (Fig. 1C). The polypeptide fragment from Cys⁶⁰ to Cys⁸² shows a zinc finger motif. However, the fragment does not form any protrusion from a globular core of the protein subunit, contrary to the typical zinc finger structure which interacts with a double-stranded DNA (20).

The electron density distribution of the enzyme crystals showed several other coordination structures, each with a central atom, that did not show any anomalous scattering for the x-rays at 1.0 Å. One of them involved an aspartate (Asp³⁶⁹) and His³⁶⁸ in subunit I, Glu¹⁹⁸ in subunit II, and an oxygen atom of water as the ligands in a distorted tetrahedral coordination (Fig. 6A). In agreement, Ferguson-Miller *et al.* discovered that His⁴¹¹ and Asp⁴¹² of *Rhodobacter sphaeroides*, which corresponds to His³⁶⁸ and Asp³⁶⁹ in beef heart enzyme, respectively, are essential for manganese binding to the enzyme at a site for which magnesium competes (21). Furthermore, electron density at this site is at a level reasonable for a magnesium atom. Thus, this site is highly likely to be a magnesium site. The magnesium site was found near (approximately 6 Å away from) two adjacent arginine residues (Arg⁴³⁸ and Arg⁴³⁹)

that faced diagonally to two propionic acid side groups of pyrroles of both hemes to form a tetrahedron involving two positively charged and two negatively charged groups. One of the ligands of the magnesium site, Glu¹⁹⁸ of subunit II, was also coordinated to Cu_A at the peptide carbonyl, suggesting an oxidation state-linked conformational change which controls the electron transfer pathways between Cu_A and Fe_a and between Fe_a and Fe_{a3} via the Arg-propionic acid system as stated above. A structural role of the magnesium for stabilizing the Cu_A site is also possible in that mutagenesis data suggest that Glu¹⁹⁸ is required for forming the Cu_A site (17). The magnesium site is located on the hypotenuse of a right-angled triangle including Fe_a, Fe_{a3}, and Cu_A with Fe_{a3}-Cu_A as the hypotenuse (Fig. 6B). The presence of zinc and magnesium in equimolar amount of heme a₃ has been reported from several laboratories (8, 22). However, the roles of these metals have not been clear. Our data clearly indicate the presence of intrinsic zinc and magnesium.

The above metal site structures are not completely consistent with the structures obtained from EXAFS. The inconsistency may be due to differences in the model used for the analysis of EXAFS data (23). The active site structures obtained here, although they resolve many controversies, require further refinement for the elucidation of the reaction mechanism of this enzyme.

REFERENCES AND NOTES

1. R. A. Capaldi, *Annu. Rev. Biochem.* **59**, 569 (1990).
2. B. G. Malmström, *Chem. Rev.* **90**, 1247 (1990).
3. G. T. Babcock and M. Wikström, *Nature* **356**, 301 (1992).
4. Ö. Einersdottir *et al.*, *Biochemistry* **32**, 12013 (1993).
5. W. S. Caughey, A. Dong, V. Sampath, S. Yoshikawa, X.-J. Zhao, *J. Bioenerg. Biomembr.* **25**, 81 (1993).
6. We follow the terminology of Kadenbach for the subunits of cytochrome oxidase [B. Kadenbach and P. Merle, *FEBS Lett.* **135**, 1 (1981); B. Kadenbach, U. Unglbauer, J. Jaraush, U. Büge, L. Kuhn-Neutwig, *Trends Biochem. Sci.* **8**, 398 (1983)].
7. O. Warburg and E. Negelein, *Biochem. Z.* **214**, 64 (1929).
8. S. Yoshikawa, T. Tera, Y. Takahashi, T. Tsukihara, W. S. Caughey, *Proc. Natl. Acad. Sci. U.S.A.* **85**, 1354 (1988).
9. S. Yoshikawa *et al.*, in preparation.

10. S. Yoshikawa, M. G. Choc, M. C. O'Tool, W. S. Caughey, *J. Biol. Chem.* **252**, 5498 (1977).
11. G. M. Baker, M. Noguchi, G. Palmer, *ibid.* **262**, 595 (1987).
12. J. P. Hosler *et al.*, *J. Bioenerg. Biomembr.* **25**, 121 (1993); B. L. Trumpower and R. B. Gennis, *Annu. Rev. Biochem.* **63**, 675 (1994).
13. B. C. Hill, *J. Biol. Chem.* **266**, 2219 (1991).
14. W. S. Caughey *et al.*, *ibid.* **250**, 7602 (1969).
15. B. F. Van Gelder and H. Beinert, *Biochim. Biophys. Acta* **189**, 1 (1969).
16. S. C. Lee and R. H. Holm, *J. Am. Chem. Soc.* **115**, 5833 (1993); A. Nanthakuman *et al.*, *ibid.*, 8513; G. Palmer, G. T. Babcock, L. E. Vickery, *Proc. Natl. Acad. Sci. U.S.A.* **73**, 2206 (1976); C. H. A. Seiter and S. G. Angels, *ibid.* **77**, 1806 (1980).
17. M. Kelly *et al.*, *J. Biol. Chem.* **268**, 16781 (1993).
18. T. Tsukihara *et al.*, *J. Biochem.* **90**, 1763 (1981).
19. P. M. H. Kroneck, W. A. Antholine, J. Riester, W. G. Zumft, *FEBS Lett.* **247**, 70 (1988); B. G. Malmström and R. Aasa, *ibid.* **325**, 49 (1993); N. J. Blackburn, M. E. Barr, W. H. Woodruff, J. van der Oost, S. de Vries, *Biochemistry* **33**, 10401 (1994); H. Bertagnolli and W. Kaim, *Angew. Chem. Int. Ed. Engl.* **34**, 771 (1995).
20. T. Hård *et al.*, *Science* **249**, 157 (1990).
21. J. P. Hosler, M. P. Espe, Y. Zhen, G. T. Babcock, S. Ferguson-Miller, *Biochemistry* **34**, 7586 (1995); M. P. Espe, J. P. Hosler, S. Ferguson-Miller, G. T. Babcock, J. McCracken, *ibid.*, p. 7593.
22. Ö. Einersdottir and W. S. Caughey, *Biochim. Biophys. Res. Commun.* **129**, 840 (1985); G. C. M. Steffens, T. Soullinam, G. Wolf, G. Buse, *Eur. J. Biochem.* **213**, 1149 (1993); M. Öblad *et al.*, *Biochim. Biophys. Acta* **975**, 267 (1989).
23. R. A. Scott, *Annu. Rev. Biophys. Biophys. Chem.* **18**, 137 (1989).
24. N. Sakabe, *J. Appl. Cryst.* **16**, 542 (1983).
25. Z. Otwinowski, DENZO. "A film processing program for macromolecular crystallography" (Yale University, New Haven, CT, 1985).
26. ———, *MLPHARE CCP4 Proc.*, p. 80 (1991) (Daresbury Laboratory, Warrington, UK).
27. D. W. Green, V. M. Ingram, M. F. Perutz, *Proc. R. Soc. London Ser. A* **225**, 287 (1954).
28. B. C. Wang, *Methods Enzymol.* **115**, 90 (1985).
29. A. T. Brunger, *Nature* **355**, 472 (1992).
30. G. Bricogne, *Acta Crystallogr. A* **30**, 395 (1974); *ibid.* **32**, 832 (1974).
31. T. A. Jones, *J. Appl. Cryst.* **11**, 268 (1978).
32. Supported in part by the Ministry of Education and Culture of Japan Grants-in-Aid for Scientific Research on Priority Area [Bioinorganic Chemistry and Cell Energetics (S.Y.), and 06276102 and 05244102 (T.T.)]; Grants-in-Aid for Scientific Research 06558102 (T.T.). The work was done with the approval of the Photon Factory Advisory Committee, the National Laboratory for High Energy Physics, Japan (proposal 91-050 and 94G-041). We thank N. Sakabe, A. Nakagawa, N. Watanabe, and S. Ikemizu for help in data collection by means of the Weissenberg camera and synchrotron radiation, Y. Morimoto for advice in computation, and S. Ferguson-Miller for the results about Mg binding site in the enzyme before publication.

3 July 1995; accepted 24 July 1995